P. M. Merifield* (*editor*)
J. M. Saari
R. W. Shorthill
R. L. Wildey
D. E. Wilhelms
R. S. Williams, Jr.

Interpretation of Extraterrestrial Imagery

Frontispiece. The multiringed basin of Mare Orientale. Lunar Orbiter IV moderate resolution photograph. Framelet width is about 90 km. Framelet orientation varies among the various Orbiter missions. (See page 489.) Note: North is at the top in this and succeeding lunar photographs. (NASA photo.)

Earth based telescopes; Photogeologic mapping of the Moon; Thermal mapping of the Moon; Lunar and planetary probes; Geologic interpretation of Lunar Orbiter photos; Photographic sensors for detecting extraterrestrial life.

(*Abstract on next page*)

Introduction

Three years have elapsed since progress in the field of space imagery has been reported on to the members of the society (Van Lopik, Merifield, *et al*, 1965), and a review of

* Chairman, Subcommittee VII, Photo Interpretation Committee, American Society of Photogrammetry, 1964–1967. Present address: Earth Science Research Corp., Santa Monica, Calif. 90405. The authors are identified in their respective sections.

some of the major projects that have been undertaken is deemed appropriate. Terrestrially based telescopic photography and infrared imagery are continuing to be utilized as fundamental tools in the study of celsetial bodies. Knowledge of the lunar and Martian surfaces has been increased many fold by imagery returned from Ranger, Surveyor, Lunar Orbiter and Mariner spacecraft. Satellite imagery of the earth is the subject of a subsequent paper to be published in this journal. Although this paper is intended to encompass the broad spectrum of the subject, it can not be considered comprehensive. Many projects have been reported elsewhere, and in such instances, the reader is referred to the appropriate literature.

ABSTRACT: *Imagery interpretation is playing an important role in the investigation of celestial bodies. Astronomers utilize terrestrially based photography in the identification and mensuration of celestial objects such as galaxies, planetary nebulae, supernova remnants and sun spots. Telescopic photographs of the Moon are being used to construct 1:1,000,000-scale maps of the lunar surface, and Earth-based infrared images of the Moon provide information on the distribution of hot spots and aid in the analysis of thermal contour maps. Surveyor photography has yielded data on the size, shape and distribution of lunar surface fragments as well as the mechanical and photometric properties of lunar soil. Interpretation of Lunar Orbiter photographs continues to provide new insight into the origin and history of lunar surface features.*

TERRESTRIALLY BASED TELESCOPES

PHOTOGRAPHIC IMAGERY IN CLASSICAL ASTRONOMY*

THE CAMERA THAT provides the astronomer with imagery is simply a large telescope in whose focal plane is placed a photographic plate. The primary use categories of the developed plate are: (1) recognition and classification of particular forms in the image detail, (2) image photometry, and, the most time-honored of all, (3) the determination of accurate relative positions of objects on the celestial sphere. The observational difficulties which confront these endeavors are dominated by the principal problems of (1) resolution and (2) radiative signal-to-noise ratio. The nearer objects are sufficiently bright that these two difficulties may be considered independently, but fainter objects, such as the outer regions of galaxies, present a situation in which the desired goals compete with one another in a direct trade-off, because the faster emulsion of a given type is always the grainier one.

Most of the well-known astronomical telescopes are sufficiently large that off-axis aberrations are of limited concern for the practical sizes of photographic plates. The classical large refracting telescopes whose design culminated in the last century in the construction of the Yerkes 40-inch and Lick 36-inch objective lenses, are usually most aberrant in chromatism and sphericity, while at sufficient distance from the optical axis astigmatism becomes important. Modern, large, fast reflecting telescopes have paraboloidal surfaces so that perfect imaging is theoretically possible until such distance from the optical axis is achieved as allows coma to quickly set in. Except for telescopes designed specifically for wide-angle imagery, much use is made of the *naturally* occurring coma-free field. When the 200-inch Hale telescope was built, at f/3.3, the coma-free field was too small for adequately precise iris-diaphragm photometry of stellar images, and a corrector lens was designed by Ross to enlarge this field (Bowen, 1960a).

The epitome of wide-angle telescopes is the true Schmidt camera, which makes use of the fact that a spherical mirror has no optical axis and cannot, therefore, if a concentrically curved focal surface is used for the photosensitive surface, show coma or astigmatism (those aberrations which depend on size of field). Only spherical aberration is left, and this can be removed by figuring a corrector plate, as an entrance pupil, as a figure of revolution based on a calculated fourth-

* Contributed by Robert L. Wildey, U. S. Geological Survey, Flagstaff, Arizona. Publication authorized by the Director, U. S. Geological Survey.

degree polynomial (Bowen, 1960b). Of course, the reflector plate *does* have an axis, but because it is not a focusing device its effects are quite weak.

The angular resolution achievable in astronomy is usually limited by the turbulence in the atmosphere as a disturbance to its wave-propagating characteristics (Stock and Keller, 1960). The air ought to act, ideally, as an optically flat filter preceding the objective. A fluctuation in density is a fluctuation in refractive index, however, and so this is not the case. The average size of the *seeing* tremor disk might be 1 to 2 seconds of arc at a reasonably good observatory site, while from three to seven nights a year it would become as small as 0.2 to 0.3 arc-sec in diameter.

Apart from *seeing*, there is a fundamental resolution limit imposed by the Fraunhofer diffraction of the objective mirror, acting as an aperture stop. But this cannot be achieved unless the primary mirror is precisely figured. And even a mirror which is initially correct can be strongly disturbed by thermal shock—or flexure through improper support (Meinel, 1960). The requisite conditions become harder to fulfill as the mirror diameter increases. Smaller mirrors can be figured to achieve consistently their diffraction limit under normal nighttime operating conditions. The diameter of diminishing returns begins to set in at about 30 inches, and a 60-inch telescope which achieves its diffraction limit is quite rare. Although the diffraction limit of the 200-inch Hale is 0.035 arc-sec, its optimum figure limit is about 0.3, whereas the U. S. Geological Survey's 30-inch telescope has a 0.18 arc-sec diffraction limit and 0.20 has been achieved in practice.

In photographic imagery, the signal-to-noise ratio in brightness comparisons depends on quantum detectivity (essentially emulsion graininess), the actual brightness level, and exposure time. Certainly a low f/ratio (usually implying a large mirror) improves the signal-to-noise ratio achieved in a certain period of time, but because of the saturation phenomenon of a photographic emulsion coupled with the importance of reciprocity failure at typical astronomical brightness levels, the faintest signal that can be detected against the sky depends only on the effective focal length of the telescope and the emulsion type itself, for a given sky background (Baum, 1962; Bowen, 1962). The f/ratio only affects the time required to reach this limit. Again because of the usual correlation with graininess, a slow emulsion and not a fast one is desirable if one can practically afford the increased observing time required to reach the minimum detectable brightness (Sandage and Miller, 1966). A typical emulsion used in observing faint sources such as faint stars, distant galaxies, and gaseous nebulae would be an Eastman Kodak type 103a or IIa emulsion, whereas for brighter objects like the Moon, a much less grainy emulsion such as 649 or even Panatomic X can be considered. One of the techniques of avoiding the trade-off between the problem of signal-to-noise (speed) and resolution (graininess) is the use of an image tube (Kron, 1966; Kron and Papiashvili, 1962) which adopts an electron-focused photo-emissive surface as an intermediary to improve the basic quantum efficiency of the photographic process.

Some of the uses of imagery for morphological classification have been: classification of galaxies into a supposed evolutionary sequence (Sandage, 1961a; Arp, 1966); distinction between distended gaseous nebulae, planetary nebulae, and supernova remnants (Abel *et al.*, 1964); distinction between open star clusters and globular clusters (Wildey, 1961); classification of sunspot groups; distinction between primary and secondary impact craters on the Moon (Shoemaker, 1962); interpretation of lunar features, such as volcanic craters, domes, sinuous rilles, and garbens; geologic mapping by surficial expression (Shoemaker and Hackman, 1962); and the identification of Martian canali.

The second category—photographic photometry of celestial imagery—is untrustworthy unless great care is taken to ensure uniformity of exposure and development and preferably to calibrate simultaneously with photoelectric observations of detailed parts of the object. The photoelectric observations are calibrated, in turn, to starts of constant luminosity, and when sufficiently comprehensive they crosscheck the overall spatial uniformity in photometric responsivity. Lunar photometry may be used to determine constraints for models of the lunar surface structure and as a lunar geologic mapping tool (Wildey and Pohn, 1964; Pohn and Wildey, 1967). Similarly, an important constraint on atmospheric models is the predicted limb-darkening of the planet in question. Stellar photometry constrains theories of stellar structure and evolution as well as the atmospheres of stars (Wildey, 1964).

The third category—astrometric photography—is responsible for both the establishment of the scale of the entire Universe outside the solar system, via measurement of stellar parallaxes as the Earth travels over

half an orbit about the Sun (Strand, 1963), and the determination of space motions of stars through measurement of angular position changes (Dieckvoss, 1963) over a period of several decades (proper motions) in combination with spectroscopic Doppler radial velocities. Although astrometric measurements provide distances only out to about 10^{15} km. (the radius of the Galaxy is of the order 10^{18} km. and the radius of curvature of the geometry of the Universe is of the order 10^{20} km.), all the myriad of distance-finding techniques telescope together in calibration, with stellar parallaxes forming the ultimate basis (Sandage, 1961b). The fundamental assumptions in astrometry are that: (1) The very faintest stars form a fixed reference system which can be used to correct field distortions, whose parallaxes and proper motions are immeasurably small because of their great distances; and (2) the center of a stellar image represents the position of the stellar point source and hence reduction of random error through many measurements is justified. Astrometric techniques are used in Earth-based selenodesy, but the limitation is much more severe because of the lack of justifiable substitutes for the aforementioned assumptions (Arthur, 1962; Wildey *et al.*, 1967).

Although the sophistication of instrumentation placed at the focal planes of telescopes has increased tremendously in the last 10 years, the fundamental tool of observational astronomy will continue to be for some time, as it has been for 75 years, the photographic plate.

Photogeologic Mapping of the Moon*

Systematic geologic mapping of the Moon from telescopic data has been carried out since 1960 by the U. S. Geological Survey. Considerable geologic information about the Moon has been accumulated, and the way prepared for unmanned Surveyor and Lunar Orbiter spacecraft missions. The purpose of lunar geologic mapping is to determine and map the stratigraphy and structure of the Moon's crust, to work out from this the sequence of events that led to the present condition of the surface, and to discover the processes by which these events took place. Fifteen colored maps of the Moon's near side at a scale of 1:1,000,000 have been published and an additional 31 are in preparation.

Geologic investigations of both the Earth and Moon are carried out by dividing the crust, which at first appears to be bewilderingly complex, into units. These units are rock bodies that seem to have a relatively uniform character over a wide lateral range and were probably laid down or emplaced in a relatively short period of time. Systematic geologic study of the Moon began when it was realized that rock units could be recognized on the Moon and placed in an age sequence through the interpretation of photographs. Recognition of age units is perhaps the most noteworthy contribution of the geologist to lunar studies, and has been the key to partly unravelling the Moon's structure, history, and crustal processes. The basic gross units are (1) the dark, relatively smooth flat mare plains, and (2) the lighter rugged cratered terra (also referred to as uplands or highlands). Almost any hypothesis of formation of these gross provinces and of craters leads to the conclusion that the maria are younger than the terrae; the maria filled depressions in the terrae as coffee fills a cup and have had less time to become cratered than the terrae.

An extensive history has been worked out by application of such reasoning in the Archimedes area (Figure 1) between the Apennine Mountains (Montes Apenninus) and the main part of Mare Imbrium (Shoemaker, 1964). The oldest material forms the rugged mountains themselves, which are part of a circular ring of mountains around a circular depression, the Mare Imbrium basin. Second in age is the light plains material that fills in around the rugged material, and third the crater Archimedes, whose rim material and secondary craters are deposited on the light plains. Next youngest is mare material, younger than Archimedes because a) the mare fills Archimedes, and b) the extensive fan of Archimedes rim material and secondary craters present on the light plains are missing on the mare. Youngest are the craters Autolycus and Aristillus, whose crater and ray pattern, being completely developed on the mare and not filled or embayed like Archimedes, show that they are younger than the mare; some rays are on the mare inside Archimedes. Thus we have five discrete rock units in an ascending age (stratigraphic) column: rugged highlands, light plains,

* Contributed by Don E. Wilhelms, U. S. Geological Survey, Menlo Park, California. Publication authorized by the Director, U. S. Geological Survey.

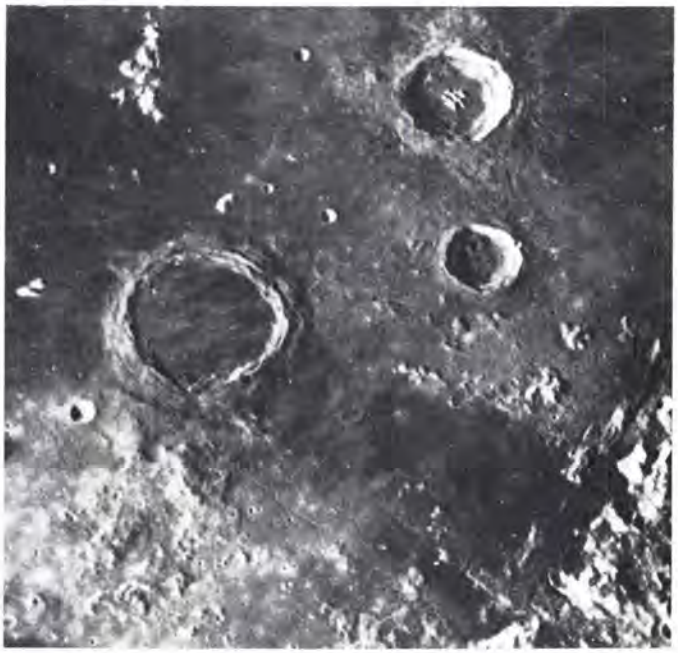

FIG. 1. Archimedes region, illustrating age sequence of lunar geologic units. The dark smooth (mare) area (upper left—northwest) is part of Mare Imbrium; part of Apennine Mountains in lower right corner. Archimedes is the large (80 km) mare-filled crater. The other two large craters are Autolycus (top) and Aristillus. One of the best Earth-based photographs ever made, taken by H. G. Herbig with the 120-inch reflector, Lick Observatory.

Archimedes materials, mare materials, young crater materials. These relations demonstrate the important fact that the mare is not only younger than the rugged terra but is enough younger to have given time for the light plains and Archimedes to form before the mare formed.

Interpretations of the origin of the lunar materials have been made from their surface characteristics and lateral distribution. These materials are concluded to be complexly interbedded layers of volcanic and impact origin. A fragmental layer forms on all exposed surfaces, its depth varying with the age of the surface.

Craters, specifically, are doubtless of both impact and volcanic origin. The craters along Hyginus rille (Figure 2) are an example of the volcanic; they are so regular in spacing and size that they must have formed by volcanic action localized along the rille (graben). Other volcanic craters are those at the tops of shieldlike domes.

The origin of craters by impact is deduced as follows: first, an explosive process is shown to have formed the craters, and second, impact is reasoned to be the explosive process. The explosive origin of Copernicus (90 km. in diameter) was demonstrated beyond reasonable doubt by Shoemaker (1962), who showed that the pattern of secondary craters around Copernicus is accounted for to the last detail by ejection of the secondary crater-producing fragments by energy from a point source within Copernicus. And in general, the large extent and radial symmetry of hummocky material (near the rimcrest), radial grooves and ridges (farther out), secondary craters, and above all of the rays that extend great distances from large young craters demonstrate an explosive origin. That the explosion was impact-produced can only be reasoned not proved, but it is difficult to conceive of the containment of sufficient volcanic energy long enough to be released all at once.

The circular mare basins also are believed to be of impact origin, judging from their great size and from resemblance of the extensive mantling deposits surrounding the basins, such as the deposit on the Apennine Mountains, to impact crater ejecta. However, the mare and light-plains materials that fill the basins and other depressions are probably volcanic, judging from their great lateral extent (and discounting unlikely origins such as water-laid sediments). Moreover, many of

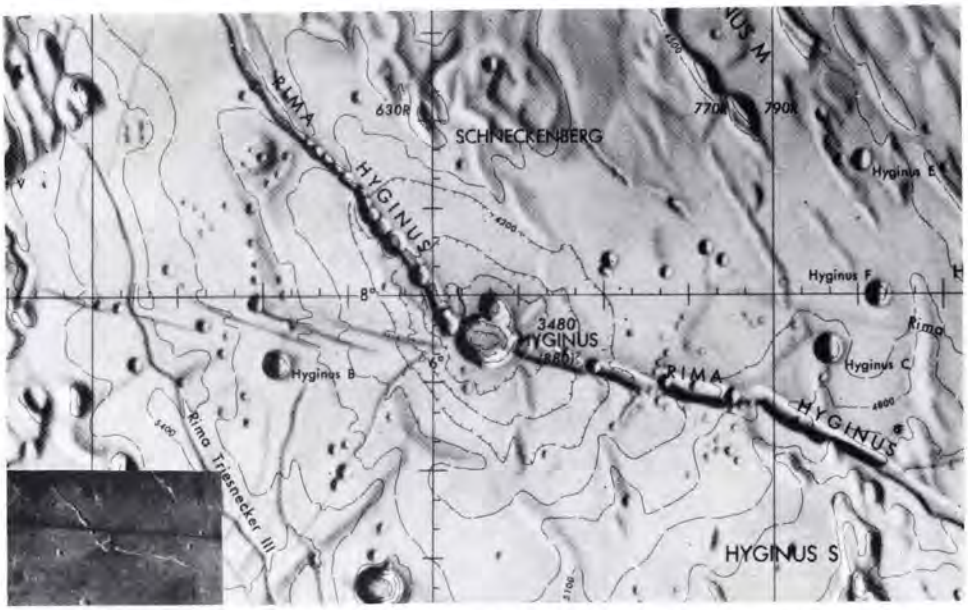

FIG. 2. Hyginus rille (Rima Hyginus). The chart (by U.S. Air Force Aeronautical Chart and Information Center) was compiled from many Earth-based photographs with critical detail added from visual telescopic observations and shows the rille and its chain of craters better than any single Earth-based photograph. The inset is from a moderate-resolution (approximately 400 m) Lunar Orbiter IV photograph and shows the rille approximately as it appears when observed visually with a large telescope on a good night. The chart and the inset include a field 175 km long.

these dark and light volcanics are believed to be flows because they terminate abruptly against higher topographic forms.

A considerable amount of information about the history and formation of the Moon's surface thus has been gathered by interpretation of telescopic photographs. Spacecraft data have confirmed some observations and interpretations and have modified others, as discussed in another section (Wilhelms, this paper).

THERMAL MAPPING OF THE MOON*

THE CONSTRUCTION OF an oscillographic thermal image of the Moon was first attempted by Sinton at the Lowell Observatory. Using a Golay cell as an infrared detector, he scanned the Moon with a resolution of 1/60 the lunar diameter. The resulting image, however, lacked sufficient detail; his results were displayed as a series of isothermal contour charts (Geoffrion, *et al.*, 1960). Recently, infrared images have been published for the full Moon and for the penumbral and umbral phase of a lunar eclipse (Saari, *et al.*, 1967) and for the third-quarter Moon (Salisbury and Hunt, 1967).

Two examples of our lunar infrared images will be presented here, one of the full Moon, and one during totality of a lunar eclipse. The measurements, made in 1963, used a mercury-doped germanium photodetector with a 10 to 12 micron filter. The Moon was scanned in a raster fashion with a resolution of about 1/200th of its diameter and the infrared signal recorded on magnetic tape (Saari and Shorthill, 1967). These measurements were made at 23 different phases through a lunation. A similar set of measurements were made during the lunar eclipse of 19 December 1964. The objective of this infrared research is to study the thermophysical properties of the lunar surface. Much of the data reduction has been done with the aid of computers; large isothermal contour charts were drawn and used for detailed quantitative analysis (Shorthill and Saari, 1965). Images reconstructed from the line-scan data were found to be useful adjuncts to our analysis because they were helpful in visualizing the global thermal patterns on the Moon.

* Contributed by J. M. Saari and R. W. Shorthill, Boeing Scientific Research Laboratories, Seattle, Washington.

FIG. 3. An enhanced infrared image of the full Moon at $23^{H}34.3^{M}$UT, 18 December 1964 (phase angle 2°16′). North is inclined at 30° to the left of vertical in both figures.

Full Moon: The infrared images were constructed by intensity modulating an oscilloscope using the recorded analog signal while applying the proper horizontal and vertical defection voltages (Saari, *et al.*, 1966). An image of the full Moon is shown in Figure 3. The variation in brightness temperatures on this image can be understood in terms of the solar radiation falling on the surface, the local inclination of the surface and its visible albedo. The incident solar radiation, which is almost completely absorbed, is reradiated at infrared wavelengths. Thus, at full Moon the brightness temperature of the subsolar point is about 398°K and decreases to approximately 320°K at the limb. Variations in local slope and changes in the visible albedo account for small differentials in brightness temperatures of the order of 10°K over the disk. Because of the large signal difference (~80°K) between the subsolar point (center) and the limb, the image was electronically enhanced to bring out these small brightness temperature differences present over the surface. The low-frequency component was removed with an appropriate filter and high-frequency emphasis was employed, so that a flat image similar to a visible photograph was obtained. This filtering technique, however, produced a deficiency in the image, in that the limbs were made over-bright.

The brighter circular regions on this image are the maria (visible albedo ~0.06), which are warmer since they absorb more of the incident solar radiation. The uplands (visible albedo ~0.12), darker on the infrared image, are cooler, as are the bright ray craters (some show up as small black dots). To the left of center and about ten scan lines in diameter is the ray crater Copernicus. Its system of bright rays is observed to be cooler than the surrounding mare material. The large circular feature (about 1/5 the lunar diameter) in the upper-left quadrant is Mare Imbrium. Variation in contrast within Imbrium may indicate different stages of lava flow as some observers have suggested. The dark outline around the right edge of Imbrium is caused by the high visible albedo of the mountains, combined with the low inclination of the Sun on the inward slopes. This same effect can be seen on several of the large craters (i.e., Copernicus).

Eclipsed Moon: The most interesting image revealed by the data is shown in Figure 4.

FIG. 4. An infrared image of the eclipsed moon at $2^{H}18.8^{M}$UT, 19 December 1964. The bright circular feature centered 30 scan lines from the bottom is the ray crater Tycho, a major hot spot. In the lower left corner the bright region in the sky is caused by thermal radiation from the telescope.

This vividly presents the heterogeneity in the thermophysical properties of the lunar surface and was obtained during the totality of the lunar eclipse. No image enhancement was needed because of the relatively large changes in signal obtained over the lunar disk. The hundreds of "hot spots" (white dots in the image) have been for the most part identified as visibly bright craters, many of which are associated with craters smaller than the resolution of the instrument (Shorthill and Saari, 1965). The image shows that the hot spots are non-uniformly distributed on the lunar hemisphere with a concentration in Mare Tranquillitatis (in the upper right quadrant on the image). In addition to the 1,000 hot spots found, portions of or all of certain maria are also observed to be thermally enhanced during the eclipse.

In conclusion, it must be stated that infrared images of the Moon furnish only qualitative information. For studying the thermophysical properties of the surface, it is necessary to do precision radiometry to obtain reliable brightness temperatures. However, infrared images, two of which have been presented here, are useful as an aid in the analysis of our large thermal contour maps and in visualizing the distribution of the hot spots.

LUNAR AND PLANETARY PROBES

SURVEYOR SPACECRAFT*

SURVEYOR I WAS successfully soft-landed on the lunar surface June 2, 1966 and returned over 11,000 television pictures to Earth. Analysis of these pictures has been described recently in this journal by Holt and Morris (1976) and Batson (1967). Surveyor II, launched September 20, 1966, crashed into the Moon on September 23, 1966.

Surveyor III soft-landed on the Moon on

* Summarized from Vrebalovich and Jaffe (1967), Shoemaker *et al.* (1967a, 1967b) and Jaffe *et al.* (1967).

April 19, 1967, and returned 6,315 television pictures. The distribution of craters and rock-like features near Surveyor III was found to be similar to that observed by Surveyor I. Blocks up to 4 m. long were visible from the spacecraft. Some of these were angular or flat; others were more rounded. Sizes of individual visible particles extended down to the 1.0 mm. resolution limit of the camera; over 85% of the exposed surface consisted of unresolved finer material. As in the Surveyor I photos, no examples were found in which a fragment seemed perched on a pedestal, as reported from the Luna IX pictures. It is believed that the pedestals reportedly observed in Luna IX pictures are illusions that are, in part, due to the lower resolution of the Luna IX pictures and to the particular conditions of illumination under which they were taken.

Television observations with color filters indicated that the Moon is gray. The local albedo of the fine-grained undisturbed surface was estimated to be $8.5\% \pm .2\%$ (Vrebalovich and Jaffe, 1967).

Surveyor III landed in a crater about 200 m. in diameter and 15 m. deep in Oceanus Procellarum. By close comparison of the Surveyor III pictures with a Lunar Orbiter III photograph of the Surveyor III landing site, it is possible to identify more than 100 craters and large blocks that are recognizable in both the Surveyor and Lunar Orbiter pictures. Because the number of these is so large, it was possible to use the information obtained from the two different sets of pictures to produce a topographic map of the crater by methods analogous to ordinary field surveying, after a solution was obtained of the orientation of the Surveyor III camera (Shoemaker, *et al.*, 1967a).

Surveyor IV, launched July 14, 1967, was unsuccessful in making a soft-landing; its retro motor exploded shortly before lunar touchdown.

Surveyor V, which soft-landed on the Moon on September 11, 1967, has returned over 19,000 pictures. The area of southwestern Mare Tranquillitatis in which Surveyor V landed appears generally similar to the sites in Oceanus Procellarum observed by Surveyors I and III (Figure 5). All three areas are fairly level, dark maria with rather similar distributions of craters and rocks. A surface layer of weakly cohesive fine particles, aggregates, and rocks is present in Mare Tranquillitatis and Oceanus Procellarum. Differences between surface layers in these maria are relatively small.

Surveyor V landed in a dimple-shaped, 9- by 12-meter rimless crater, which is the largest member of a small chain of rimless craters; a parallel row of very small craters also occurs within the large crater. On the basis of its shape and the alinement of small associated craters, the crater in which Surveyor V landed may have been formed by drainage of surficial fragmental debris into a northwest-trending fissure.

Observations of block-rimmed craters, relatively nearby, indicate that the local thickness of the layer of fragmental debris with low cohesion is not more than 5 meters. The walls of the Surveyor V crater provide exposures of the upper meter of this debris layer. Different types of fragments are revealed in the pictures of the debris dislodged from these walls during the spacecraft landing and in the pictures of the undisturbed parts of the walls. The types of fragments include (1) bright, angular objects, which are inferred to be pieces of dense rocky material; (2) dark, rounded objects, which are probably aggregates of very fine-grained particles; and (3) dark, lumpy objects, which appear to be aggregates of aggregates. The aggregate character of some of the loose, ejected fragments is well demonstrated by the presence of bright, angular chips set in a dark, fine-grained matrix.

The estimated normal albedo (normal luminance factor) of the undisturbed parts of the lunar surface near Surveyor V is 7.9 ± 1.0 percent, somewhat lower than that observed at the Surveyor III landing site. Debris ejected on the lunar surface in front of the footpads has a normal albedo of 7.5 ± 1.0 percent, which is only about one-twentieth lower than the albedo of the undisturbed surface, but is similar to the albedo of the material disturbed by the footpads at the Surveyor III landing site (Jaffe, *et al.*, 1967, Shoemaker, *et al.*, 1967b).

Surveyors VI and VII, the final two Surveyor spacecraft, have made successful soft landings on the Moon and have returned high quality television pictures as well as information about the composition of the lunar surface from magnetic and alpha backscattering experiments. Analysis of the data from these most recent flights is currently in progress.

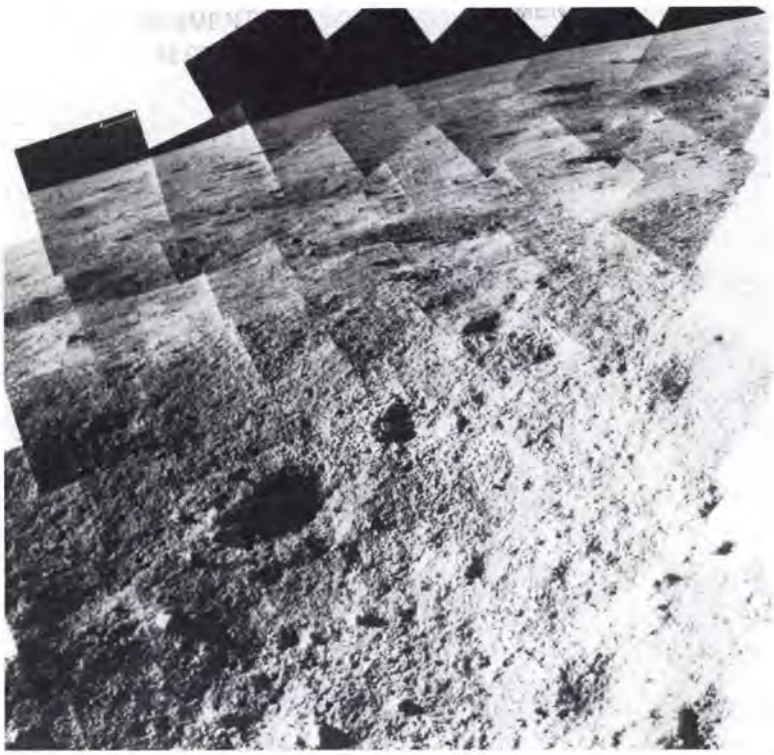

FIG. 5. Mosaic of narrow-angle pictures from Surveyor V showing the northwest wall of the crater in which the spacecraft is located and the far field beyond the rim of the crater extending to the horizon. (NASA photo.)

GEOLOGIC INTERPRETATION OF LUNAR ORBITER PHOTOGRAPHS*

THE EXTRAORDINARILY successful Lunar Orbiter project has produced a rich photographic data bank that is greatly increasing geologic knowledge of the Moon and will continue to do so for years to come. Because of the wide areal coverage—nearly complete for the whole Moon at 500 meters resolution or better, nearly complete for the Earth-facing side at 70 to 200 meters and very extensive at 1 to 20 meters—Orbiter photos serve as the context in which to place data from spacecraft missions such as the Surveyor and the projected manned Apollo missions. This discussion will briefly show how Orbiter refines the basic geological framework interpreted by Earth-based telescopic means, mainly by the U. S. Geological Survey, discussed in an earlier section (Wilhelms, this article). Quantitative photogrammetric results, still preliminary, will not be discussed.

* Contributed by Don E. Wilhelms, U. S. Geological Survey, Menlo Park, California. Publication authorized by the Director, U. S. Geological Survey.

Five Lunar Orbiter missions flew successfully out of five attempted, a remarkable record, especially since they flew nearly on schedule. Lunar Orbiter I (August 1966) photographed 9 potential Apollo landing sites selected on the basis of Earth-based photographs and telescopic observations in the equatorial belt; it also photographed a number of supplementary sites. During the photographic portion of the mission, periapsis (nearest approach) fell near the Apollo belt and averaged 52 km. altitude, and apoapsis (highest point of orbit) came on the far side and averaged 1,850 km. altitude. Resolution of about 8 meters was achieved on the Earth-side medium resolution photographs, but the failure to achieve the proper image-motion compensation for the high-resolution system caused unacceptable smear of the high-resolution frames—the only significant failure of the entire program. However, excellent photographs were obtained of the far side, including the famous frames with the Earth in the background. Lunar Orbiter II (Novem-

ber 1966), a similar mission, was almost completely successful and contributed the most of all missions to specification of Apollo sites, 5 of the 13 photographed becoming prime sites. It also contributed the famous oblique photograph of the crater Copernicus. Mission III (February 1967) differed slightly from the first two in that the orbit was inclined 21° to the equator in order to explore additional sites, including several photographed at an oblique angle because of the success of the Mission II Copernicus oblique. Mission III added 3 prime Apollo sites and many other sites of scientific interest; its only failure was in lost frames in some of the eastern sites.

These three missions filled most of the direct Apollo requirements and left the remaining two largely for scientific purposes (which of course also apply to Apollo). Mission IV (May 1967) was of a type entirely different from the first three and unforeseen in the design of the spacecraft. Its altitude (approximately 2,700 km. periapsis, 6,100 km. apoapsis) and orbit inclination (85°) allowed it to survey the entire front side of the Moon, which it did with stunning success, except for a fogged strip 10° wide in the east, in the face of greater difficulties than faced in any other mission. This is the single mission that, because of its wide coverage, will probably prove to have the greatest ultimate value to lunar studies, although its value would have been greatly reduced without the earlier and later high-resolution missions. The greatest achievement of Mission IV was perhaps the photograph of the Orientale basin (Frontispiece), taken near the end of the photo mission. Mission V (August 1967—only a year after Mission I) was another largely scientific mission and an extraordinarily productive and successful one, the most nearly flawless of all Lunar Orbiter missions despite the fact that it, too, flew an 85° orbit, which the spacecraft was not designed for. It supplemented the other Apollo-oriented missions by adding another possible site and by providing high-resolution stereoscopic coverage for four prime Apollo sites selected by earlier missions.

Gross geologic (rock or age) units are recognized on Earth-based photographs and finer-scale ones on Orbiter photographs. The Orbiter-derived units commonly are composed of surficial materials that show age relations opposite to those among the gross units on which they are developed. For example, telescopic studies of the Flamsteed region, landing site of Surveyor I, clearly indicated age relations like those at Archimedes, where young mare material embays and fills an old crater, but Orbiter photographs of the Flamsteed ring (Flamsteed P) produced a surprise that led to new knowledge of lunar surface processes. Orbiter I showed a convex *moulding* all around the Flamsteed ring that is clearly superposed on the mare and so is younger (Figure 6). This relation could be interpreted to mean that the ring itself was younger than the mare and therefore was some sort of volcanic extrusive overlying a ring dike (O'Keefe, 1967); but since such *mouldings* are also present around many contacts of mare with rugged objects, including many diverse forms difficult to explain by volcanism, the more reasonable hypothesis is that the surface material on old terrain is a mobile fragmental layer that migrates downslope through the effects of gravity in a lunar manifestation of the process called mass wasting. Such mass wasting probably explains the relative paucity of small craters on slopes relative to plains, also the reverse of what is expected from the gross age relations. These observations (1) set limits on the engineering properties of lunar surface materials, and (2) show that astronauts will seldom find in-place rock outcrops to sample in old terrain but will easily be able to sample the average composition of a rugged terra by sampling the float at its base.

From the apparent abrupt termination of mare material against terra observed telescopically, it was early reasoned that the mare consisted of volcanic flows and the wide areal extent of the presumed flows suggested, through analogy with terrestrial rocks, either basalt or ash-flow tuff. Surveyor V and VI observations apparently indicate a basaltic composition for the maria, and Orbiters IV and V have confirmed that flows are present by photographs of very clear flow fronts in Mare Imbrium (Figure 7) (previously indicated but not proved in excellent telescopic photographs). The presence of more than one flow indicates an extended and complicated history of mare emplacement, as expected from the delayed filling of Mare Imbrium deduced telescopically and from experience on Earth, where very little happens cataclysmically.

Many events on the Moon do happen cataclysmically, in particular the formation of many craters, as discussed in an earlier section (Wilhelms, this paper). Many geologists, however, have resisted this fact, presumably because of their experience with Earth geology—or what seemed to be their

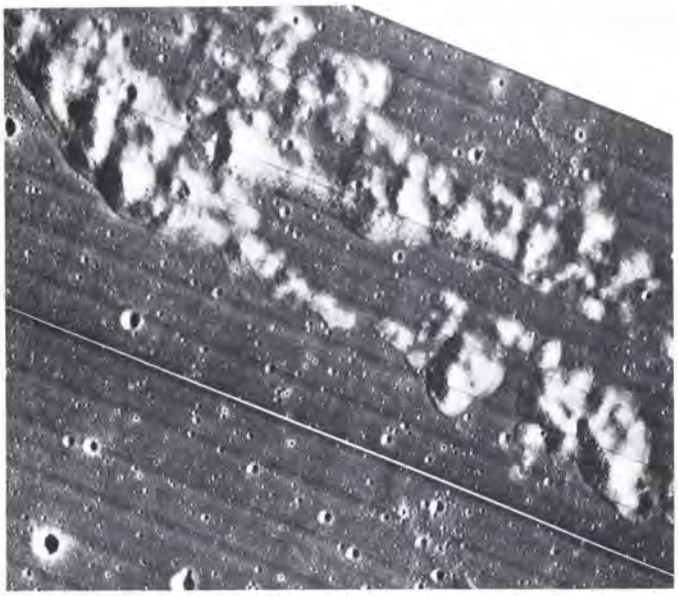

FIG. 6. Part of the Flamsteed ring, showing convex *mouldings* at base of slopes. Lunar Orbiter III moderate resolution photograph; site was also photographed by Orbiter I and the ring appears in the distance in Surveyor I photographs. Framelet width is about 1.8 km (NASA photo.)

experience. As the impact origin of many lunar craters is being demonstrated, more and more impact craters are being found on Earth as well. The Moon, however, is still where the big ones are found. Impact craters range in size from tiny ones observed on high-resolution Orbiter photographs through telescopically observed craters such as Copernicus to mare basins such as Imbrium and Orientale (to be discussed below).

It must be emphasized that many of the smaller craters have long been believed by all but the most fanatic impact proponents to be volcanic (or more generally, internal) in origin, and this belief has been confirmed beyond a shadow of a doubt by Orbiter photographs. An example is the craters along Hyginus rille, discussed in the section on mapping (Wilhelms, this paper), known and interpreted as volcanic in origin before Orbiter; this origin was only confirmed by Orbiter.

Other fascinating features of internal origin are sinuous rilles, river-like objects

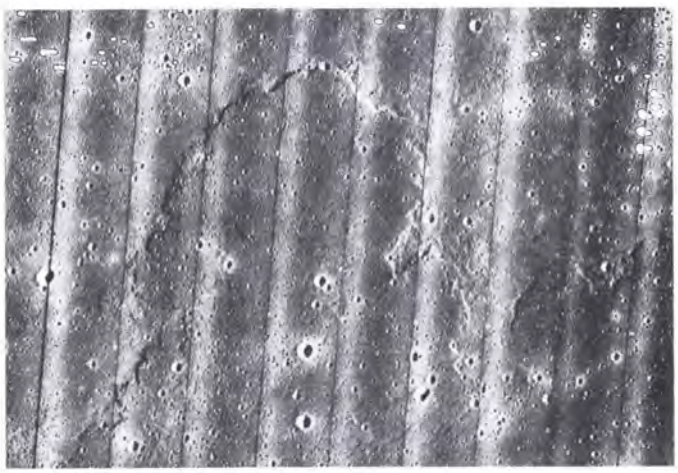

FIG. 7. Lobate flows in Mare Imbrium. Lunar Orbiter V moderate resolution photograph. Framelet width is about 5 km. (NASA photo.)

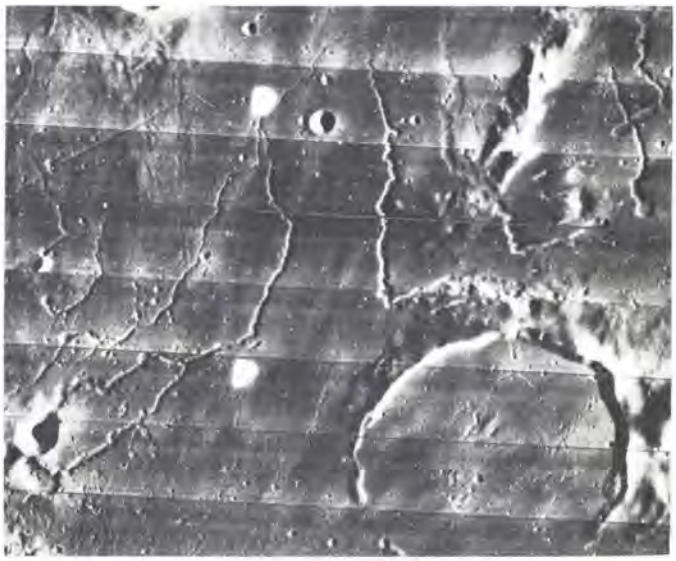

FIG. 8. Sinuous rilles near the partly buried crater Prinz. Lunar Orbiter IV high resolution photograph. Framelet width is about 14 km. (NASA photo.)

which, with few exceptions, had been too poorly seen before Orbiter to establish their mode of formation, now known to be by some flow mechanism still not understood in detail, and not by faulting (Figure 8).

Another way in which Orbiter photographs help interpret Earth-based observations should be mentioned. Several craters, crater chains and other objects were selected to be photographed by Orbiter partly because they show an anomalously high signal in the thermal region of the infrared at eclipse. One interpretation of this anomalous signal was that an insulating layer apparently present over most of the Moon was lacking and fresh rock might be exposed, and indeed high-resolution Orbiter photographs show many large fresh rock fragments at every such infrared anomaly photographed. Such fresh rock was sought by Orbiter because it will provide valuable samples to be collected by astronauts.

A final lunar feature to be discussed here is perhaps the most spectacular of all photographed by Lunar Orbiter, the Mare Orientale basin (Frontispc.), barely reached by Lunar Orbiter IV before its picture-taking ability gave out. The importance of Orientale in lunar geologic studies is that it is the freshest object at the upper end of the impact size scale—a mare basin, that is, a large circular crater surrounded by multiple rings and partly filled by mare material. (Orbiter photographs of the far side of the Moon show structural basins that are similar but lack mare filling.) Fresh exposures in Orientale of structures and geologic units that are eroded and covered in older basins show what is to be expected in the other basins, such as Imbrium. Four rings of peaks surround Orientale, and interestingly similar but more subdued and more deeply covered ones occur in the other basins—in about the same spacing. The inner ring of islands in Imbrium was once thought to ring an inner deep basin like, say, the crater Copernicus; now it is seen that the inner basin probably lies somewhat inside this ring and is relatively shallow. The third ring corresponds to peaks covered by Archimedes rim material, as discussed in an earlier section (Wilhelms, this paper).

The continuity and regularity of the rings of Orientale and therefore Imbrium show that each of these craters is a unified structure whose origin centered about a point—an origin easily explained by impact (of an object only a few miles in diameter) but difficult to explain by an internal mechanism; a pre-caldera dome, for example, would have to have been of enormous height to collapse and form the present ring structure. The surface materials also suggest impact origin. Most interesting is the outer ridged and grooved material first seen in Orientale (McCauley, 1967b). Comparison of ring structures between basins shows that this corresponds in position to material on the flanks of the Apennine Mountains, long

FIG. 9. Floor of Orientale basin including young probable volcanic crater (lower right quadrant) and part of young probable impact crater (upper left). Lunar Orbiter IV moderate resolution photograph. Framelet width is about 12 km. (NASA photo.)

believed to be impact ejecta from the giant Imbrium basin-crater. The Orientale material, to have such streaked texture, must have been emplaced by a great outward rush of material such that could hardly have been produced by volcanism; even though the details of texture around the older eroded Imbrium are not clear, the analogy with Orientale supports the impact origin of Imbrium.

Orientale's freshness provides an additional opportunity to interpret origins from photographs. Since the features superposed on the young Orientale are known to be young, the crater shown in lower right of Figure 9 must be young; but it lacks the hummocky terraces, radial ridges and grooves, and secondary craters of the large craters discussed above and of the crater near it (upper left corner of photograph). Therefore, with the variable of age better known than for other craters, a caldera origin is here very strongly supported and criteria for recognition of other calderas can be developed (McCauley, 1967b).

In summary, it should be clear from the foregoing discussion that no single, simple origin of lunar features can be invoked to explain all lunar features; volcanism and impact have both played a role. This fact should always have been assumed, and was well demonstrated by Earth-based means, but it has been spectacularly confirmed by the highly successful Lunar Orbiter program. It remains to establish the relative proportions of impact and volcanic features and to determine exactly how these two processes, along with mass wasting, radiation, tectonism, and other processes, have shaped the surface of the Moon and at what time in the history of the Earth-Moon system it all took place. Photographs from Lunar Orbiter and those to be taken by future orbiting spacecraft will be the principal tool for doing this. Data acquired by other means can be fitted to the framework provided by the Orbiter missions, and Orbiter will show the way for manned exploration to sample localities likely to yield diagnostic material.

PHOTOGRAPHIC SENSORS FOR THE DETECTION OF PAST AND PRESENT EXTRATERRESTRIAL LIFE*

PRELIMINARY WORK BY Air Force Cambridge Research Laboratories' Terrestrial Sciences Laboratory in the continuing investigation of the application of remote sensors for geological research has suggested two films and spectral regions amenable for the possible detection of past and present life on other planetary surfaces. The two types of photography are ultraviolet and false color (color infrared, camouflage detection).

* Contributed by R. S. Williams, Jr., Air Force Cambridge Research Laboratories, Bedford, Massachusetts.

Ultraviolet photography in the 3,900Å–4,450Å spectral region is accomplished by using Kodak 5424 film with Wratten 36 and 47B filters. Carbonates (limestones, etc.) have a higher reflectivity in this spectral region than any other common rock. On Earth, carbonates are a ubiquitous sedimentary rock. Large deposits almost invariably contain fossils of marine organisms, and most large carbonate deposits were formed in a marine environment. Extensive areas of carbonate exposure on other planetary surfaces would strongly suggest former

oceans and the presence of aqueous organisms.

False color photography was specially developed to differentiate, by color change, between living flora and ersatz flora (camouflage). False color photography is obtained with Kodak 8443 film with a Wratten 12 filter plus an emulsion balance filter. The spectral region covered lies between approximately 5000Å and 8500Å. Nonliving matter on Earth is recorded as a bluish green color. Living flora from higher order vascular plants to lower order lichens and algae are recorded as a reddish-orange color. False color photography is an accurate diagnostic tool in differentiating between living and non-living matter on the Earth's surface.

Bibliography

Abel, G. O., Aller, L. H., Czyzak, S., Henize, K. G., Kaler, J. B., Liller, W., Minkowski, R., Munch, G., O'dell, C. R., 1964, "Planetry Nebulae—A Symposium in Honor of Dr. Ira S. Bowen, May 25, 1964," *Publications of the Astronomical Society of the Pacific*, Vol. 76–77, No. 451–454.

Arp, H. C., 1966, "Atlas of Peculiar Galaxies," *Astrophysical Journal Supplements*, Vol. XIV, No. 123.

Arthur, D. W. G., 1962, "On the Problems of Selenodetic Photogrammetry," *International Astronomical Union Symposium No. 14*, Chapter 12, Academic Press, New York.

Batson, R. M., 1967, "Surveyor Spacecraft Television Photogrammetry," Photogrammetric Engineering, Vol. XXXIII, p. 1365–1372.

Baum, W. A., 1962, "The Detection and Measurement of Faint Astronomical Sources," Astronomical Techniques (Ed. W. A. Hiltner) Chapter 1, University of Chicago Press, Chicago.

Bowen, I. S., 1960a, "The 200-Inch Hale Telescope," Telescopes, (Ed. G. P. Kuiper and B. M. Middlehurst), Chapter 1, University of Chicago Press, Chicago.

Bowen, I. S., 1960b, "Schmidt Cameras," Telescopes, (Ed. G. P. Kuiper and B. M. Middlehurst), Chapter 4, University of Chicago Press, Chicago.

Bowen, I. S., 1962, "Spectrographs," Astronomical Techniques, (Ed. W. A. Hiltner), Chapter 2, University of Chicago Press, Chicago.

Dieckvoss, W., 1963, "Photographic Proper Motions," Basic Astronomical Data, (Ed. K. A. Strand), Chapter 4, University of Chicago Press, Chicago.

Geoffrion, A. R., Korner, M., and Sinton, W. M., 1960, "Isothermal Contours of the Moon," *Lowell Obs. Bull. 5*, 1–15.

Holt, H. E. and E. C. Morris, 1967, "Interpretation of Surveyor I Lunar Photos," Photogrammetric Engineering, Vol. XXXIII, p. 1352–1362.

Jaffe, L. D. *et al*, 1967, "Principal Scientific Results, Surveyor V, A Preliminary Report," National Aeron. and Space Admin., NASA SP-163, p. 1–2.

Kron, G. E., and Papiashvili, I. I., 1962, "Progress on the Lick-Stromolo Image Tube," *Publications of the Astronomical Society of the Pacific*, Vol. 74, No. 441, p. 404.

Kron, G. E., 1966, "Image Tubes," Advances in Electronics and Electron Physics, Vol. 22A, (Ed. J. D. McGee, E. Mullan, and E. Kahan), p. 59, Academic Press, New York.

Levin, Viele and Eldrenkamp, "The Lunar Orbiter Missions to the Moon," *Scientific American*, May, 1968.

McCauley, J. F., 1967a, "The Nature of the Lunar Surface as Determined by Systematic Geologic Mapping," in *Mantles of the Earth and Terrestrial Planets*, New York and London, John Wiley & Sons, p. 431–460.

McCauley, J. F., 1967b, "Geologic Results from the Lunar Precursor Probes," Am. Inst. Aeronautics and Astronautics, AIAA Paper No. 67–862, 8 p.

Meinel, A. B., 1960, "Design of Reflecting Telescopes," Telescopes, (Ed. G. P. Kuiper and B. M. Middlehurst), Chapter 3, University of Chicago Press, Chicago.

O'Keefe, J. A., Lowman, P. D., Jr., and Cameron, W. S., 1967, "Lunar Ring Dikes from Lunar Orbiter I," *Science*, Vol. 155, No. 3758, p. 77–79.

Pohn, H. A., and Wildey, R. L., 1967, "A Photoelectric-Photographic Map of the Normal Albedo of the Moon," U. S. Geological Survey Misc. Geol. Inv. Map, in press.

Saari, J. M., Shorthill, R. W., and Deaton, T. K., 1966, "Infrared and Visible Images of the Lunar Surface During the Eclipsed Moon of December 19, 1964, *Icarus 5*, 635–659.

Saari, J. M., and Shorthill, R. W., 1967, "Isothermal and Isophotic Atlas of the Moon: Contours through a Lunation," NASA Contract Report NASA CR-855.

Salisbury, J. W., and Hunt, G. R., 1967, "Infrared Images: Implications for the Lunar Surface," *Icarus 7*, 47–58.

Sandage, A. R., 1961a, *The Hubble Atlas of Galaxies*, Carnegie Publications, Washington, D. C.

Sandage, A. R., 1961b, "The Ability of the 200-Inch Telescope to Discriminate Between Selected World Models," *Astrophysical Journal*, Vol. 133, No. 2, pp. 355–392.

Sandage, A. R., and Miller, W. G., 1966, "A Search for a Cluster of Galaxies Associated with 3c 48 Using the Kodak Special Plate Type 087-01," *Astrophysical Journal*, Vol. 144, No. 3, pp. 1238–1239.

Shoemaker, E. M., 1962, "Interpretation of Lunar Craters," in Kopal, Zdenek, ed., *Physics and Astronomy of the Moon*, New York, N. Y., Academic Press, p. 283–359.

Shoemaker, E. M., 1964, "The Geology of the Moon," *Sci. American*, Vol. 211, No. 6, p. 38–47.

Shoemaker, E. M. *et al.*, 1967a, "Television Observations from Surveyor III, Surveyor III, a Preliminary Report," National Aeronautics and Space Administration, NASA SP-146, p. 9–59.

Shoemaker, E. M. *et al.*, 1967b, "Television Observations from Surveyor V, Surveyor V, a Preliminary Report," National Aeronautics and Space Administration, NASA SP-163, p. 9–42.

Shoemaker, E. M., and Hackman, R. J., 1962, "Stratigraphic Basis for a Lunar Time Scale," *International Astronomical Union Symposium No. 14*, Chapter 23, Academic Press, New York.

Shorthill, R. W., and Saari, J. M., 1965, "Nonuniform Cooling of the Eclipsed Moon: a Listing of Thirty Anomalies," *Science 150*, p. 210–212.
Shorthill, R. W., and Saari, J. M., 1967, "Radiometric and Photometric Mapping of the Moon Through a Lunation," *Ann. N. Y. Acad. Sci. 123*, Art. 2, p. 722–739.
Stock, J., and Keller, G., 1960, "Astronomical Seeing," Telescopes, (Ed. G. P. Kuiper and B. M. Middlehurst), Chapter 9, University of Chicago Press, Chicago.
Strand, K. A., 1963, "Trigonometric Stellar Parallaxes," Basic Astronomical Data, (Ed. K. A. Strand), Chapter 6, University of Chicago Press, Chicago.
Trask, N. J. and L. C. Rowan, 1967, "Lunar Orbiter Photographs: Some Fundamental Observations," *Science*, Vol. 158, p. 1529–1535.
Van Lopik, J., P. M. Merifield, *et al.*, 1965, "Photo Interpretation in the Space Sciences," PHOTOGRAMMETRIC ENGINEERING, Vol. XXXI, p. 1060–1075.
Vrebalovich, T. and L. Jaffe, 1967, "Summary of Results, Surveyor III, a Preliminary Report," National Aeronautics and Space Administration, NASA SP-146, p. 1–2.
Wildey, R. L., 1961, "The Color-Magnitude Diagram of 47 Tuc," *Astrophysical Journal*, Vol. 133, No. 2, pp. 430–437.
Wildey, R. L., 1964, "The Stellar Content of h and chi Persei-Cluster and Association," *Astrophysical Journal Supplements*, Vol. VIII, No. 84.
Wildey, R. L., and Pohn, H. A., 1964, "Detailed Photoelectric Photometry of the Moon," *Astronomical Journal*, Vol. 69, No. 8, pp. 619–634.
Wildey, R. L., Schlier, R. E., Hull, J. A., and Larsen, G., 1967, "An Operational Theory of Laser Radar Selenodesy," *Icarus*, Vol. 6, No. 3, in press.

Bibliography of Computer Programs

The ASP bibliography of computer programs has been updated by the Committee on Computational Photogrammetry, and a listing of the contents is available at the American Society of Photogrammetry, 105 N. Virginia Ave., Falls Church, Va. 22046.

When it was originally compiled, this bibliography was limited strictly to those computer programs involving photogrammetry. However, in updating the contents, the Committee has broadened the scope to include many programs which might be used in support of photogrammetric programs. As an example, programs have been included which convert latitudes and longitudes into grid coordinates, and vice versa.

The bibliography has been compiled with the intent of reducing computer programming costs and man-hours by keeping photogrammetrists informed of existing programs. The listing reveals that considerable amounts of time and money are lost each year through duplication of efforts. The enthusiastic response and assistance which the Committee has received in updating the list (as compared with the response during the original compilation) indicate that photogrammetrists are becoming aware of the savings possible.

If you have computer programs which you would like to include in this bibliography, or if you would like additional information concerning it, please contact the Society.

Articles for Next Month

Dr. J. M. Anderson, Block Triangulation by ISP Commission III.
Dr. Sidney Bertram, The UNAMACE and the Automatic Photomapper.
J. M. Burnham and *P. R. Josephson*, Color Plate Metric Stability.
C. E. Olson, L. W. Tombough, H. C. Davis, Inventory of Recreation Sites.
J. T. Parry, W. R. Cowan, J. A. Heginbottom, Color for Coniferous Forest Species.
F. B. Silvestro, Object Detection Enhancement.
Dr. B. Shmutter, Triangulation with Independent Models.
Prof. J. Vlcek, Systematic Errors of Image Coordinates.
Paul R. Wolf, Trilaterated Photo Coordinates.